Check for updates

PAIN

A thalamo-amygdalar circuit drives female vulnerability to chronic pain after early-life stress

Anna Maria Borruto[1,2]†, Tabea Kohlund[1]†, Lukas Rettig[1]†, Martin von Renesse[1]†, Christian Alexander Hammer[1]†, Nikolas Leonhardt[1], Barbara Kurpiers[1], Claudia Calpe-López[2], Luca Benn[1], Hans-Christoph Friederich[3]‡, Thomas Kuner[1], Rainer Spanagel[2]‡, Sebastian Wieland[1,3]‡*

Childhood adversity increases the risk of chronic pain and anxiety later in life, particularly in women, yet the neural mechanisms linking early-life stress to adult vulnerability remain elusive. Here, we show that social isolation and nerve injury interact to amplify activity-dependent synaptic gain and anticipatory recruitment of the paraventricular thalamus-to–central amygdala pathway in female, but not male, mice. This female-specific circuit sensitization enhances mechanical hypersensitivity and avoidance behaviors in adulthood. Chemogenetic pathway inhibition selectively rescued these behaviors when stress and injury co-occurred, whereas sustained and phasic pathway activation triggered mechanical hypersensitivity and avoidance, respectively. Together, these findings uncovered a latent thalamo-amygdalar synaptic gain state that is unmasked by a subsequent injury and transforms early-life stress into female-specific vulnerability to chronic pain and anxiety-like avoidance.

Comorbid anxiety disorders in chronic pain patients represent a major clinical challenge, reducing treatment efficacy through pain-related fear and avoidance behavior (*1*–*3*). Early-life stress (ELS), including childhood abuse and deprivation, increases the lifetime risk of developing both chronic pain (*4*) and anxiety (*5*), particularly in women (*6*, *7*). This female vulnerability often remains clinically silent for years and becomes manifest only after subsequent injury (*8*, *9*). However, the circuit mechanisms underlying this latent susceptibility remain unknown. The heterogeneity of ELS and the long latency to adult disease onset complicate causal inference in human studies, underscoring the need for mechanistic animal models.

Rodent studies show that ELS increases avoidance and hyperalgesia with sex-dependent effects (*10*–*13*). However, the neural circuitry through which ELS and subsequent injury converge to produce persistent network dysfunction remains unknown. Both early-life and acute stressors (*14*, *15*) activate the paraventricular thalamus (PVT), which regulates salience-driven behavior during motivational conflict (*16*, *17*). Through projections to the central amygdala (CeA), the PVT influences defensive behavior, fear memory, and nociceptive processing (*14*, *18*–*23*). In humans, anticipation of threat or pain also activates the midline thalamus and CeA (*24*, *25*). Together, these findings position the PVT→CeA pathway as a candidate circuit linking ELS to maladaptive pain and avoidance states (*26*–*28*). Here, we tested whether ELS primes the PVT→CeA pathway to create a latent vulnerability state that selectively drives hyperalgesia and anxiety-like avoidance in females after a subsequent injury.

[1]Department for Functional Neuroanatomy, Institute for Anatomy and Cell Biology, Heidelberg University, Heidelberg, Germany. [2]Institute for Psychopharmacology, Central Institute of Mental Health, Medical Faculty Mannheim, Mannheim, Germany. [3]Department for General Internal Medicine, Psychosomatics and Psychotherapy, Medical Faculty Heidelberg and University Clinic Heidelberg, Heidelberg, Germany. ***Corresponding author. Email: sebastian.wieland@med.uni-heidelberg.de** †These authors contributed equally to this work. ‡German Center for Mental Health (DZPG), Partner Site Mannheim-Heidelberg-Ulm, Germany.

Stress-injury interaction drives female-specific amplification of chronic pain and avoidance

To study the interaction between ELS and a subsequent nerve lesion, we combined postweaning social isolation (SI; initiated on postnatal day 21) with spared nerve injury (SNI; during late adolescence) in male and female mice and assessed long-term behavioral outcomes (Fig. 1A). In addition to mice with SI and SNI (SI+SNI mice), we included sham-operated SI-only, group-housed SNI-only, and sham-operated control (ctrl) mice to assess individual and interactional effects (Fig. 1B). SI increased mechanical withdrawal sensitivity in both sexes (Fig. 1D). Although SI-only females showed a transiently greater response during late adolescence (Fig. 1C), this difference resolved by week 4 after sham surgery (fig. S1E), indicating similar long-term pronociceptive effects of SI in males and females (Fig. 1, E and F). SNI during late adolescence induced mechanical hypersensitivity in both sexes (Fig. 1, E and F), but this response was less pronounced in SNI-only females than in males (fig. S1, A to D). Consistent with prior reports (*29*), this difference was absent when SNI was performed in adulthood (fig. S1, F and G), suggesting age-dependent modulation of neuropathic pain expression in females (*30*, *31*). Next, three-way analyses of variance (ANOVAs) revealed that SI persistently amplified neuropathic hypersensitivity in females at all examined time points (Fig. 1F). By contrast, SI did not modulate neuropathic hypersensitivity in males (Fig. 1E). The female-specific SI × SNI interaction was reproducible across experimenters and laboratories and reflected a greater SI-induced increase in withdrawal relative to SNI-only females, rather than lower baseline SNI responses (fig. S1, I to K). Thermal sensitivity in the cold-plate test was unaffected by SI in either sex (fig. S1H), indicating modality specificity. To assess spontaneous pain-related behavior, we performed automated gait analysis during voluntary locomotion in female ctrl, SNI-only, and SI+SNI mice. Running speed and stride length remained unchanged, whereas SNI produced persistent ipsilateral limb guarding, shown by altered weight bearing and swing parameters, with SI+SNI exerting additional effects (fig. S2). To determine whether SI also enhances affective-motivational aspects of pain, we assessed escape behavior in the place escape/avoidance paradigm (*32*) 12 weeks after SNI surgery in females (fig. S3A). SI+SNI females entered the aversive bright compartment more frequently and spent more time there than SNI-only females (fig. S3, B and C), indicating an increased drive to escape from injured paw stimulation. Thus, SI enhances sensory and affective-motivational dimensions of neuropathic pain in females.

To investigate whether SI exacerbates avoidance in chronic neuropathic pain, we assessed approach-avoidance conflict using the open field test (OFT), light-dark box (LDB), and novelty-suppressed feeding (NSF). All assays depend on active exploration, yet neither SI nor SNI reduced locomotor activity in male or female mice (fig. S4, A and B). In the OFT, exploratory behavior did not differ between groups (Fig. 1, G and H). In males, SI increased avoidance in the NSF, but SNI did not further exacerbate avoidance (Fig. 1, I, K, and M). In females, SI+SNI reduced exploration of the light compartment in the LDB and selectively increased avoidance in the NSF compared with the ctrl, SI-only, and SNI-only groups (Fig. 1, J, L, and N). A sex × SI × SNI interaction was only observed in the NSF. In parallel, home-cage feeding latency and total food consumption remained unchanged in both sexes (fig. S4, E to H), suggesting that avoidance in the NSF is driven by exposure to the anxiogenic environment rather than altered motivation. To assess global behavioral state changes, automated home-cage monitoring revealed that SI+SNI increased locomotion and rearing but decreased grooming in both sexes (fig. S5), consistent with hypervigilant arousal. Together, these data indicate that ELS interacts with nerve injury to selectively amplify chronic neuropathic pain and conflict-driven avoidance in females.

Downloaded from https://www.science.org on November 24, 2026

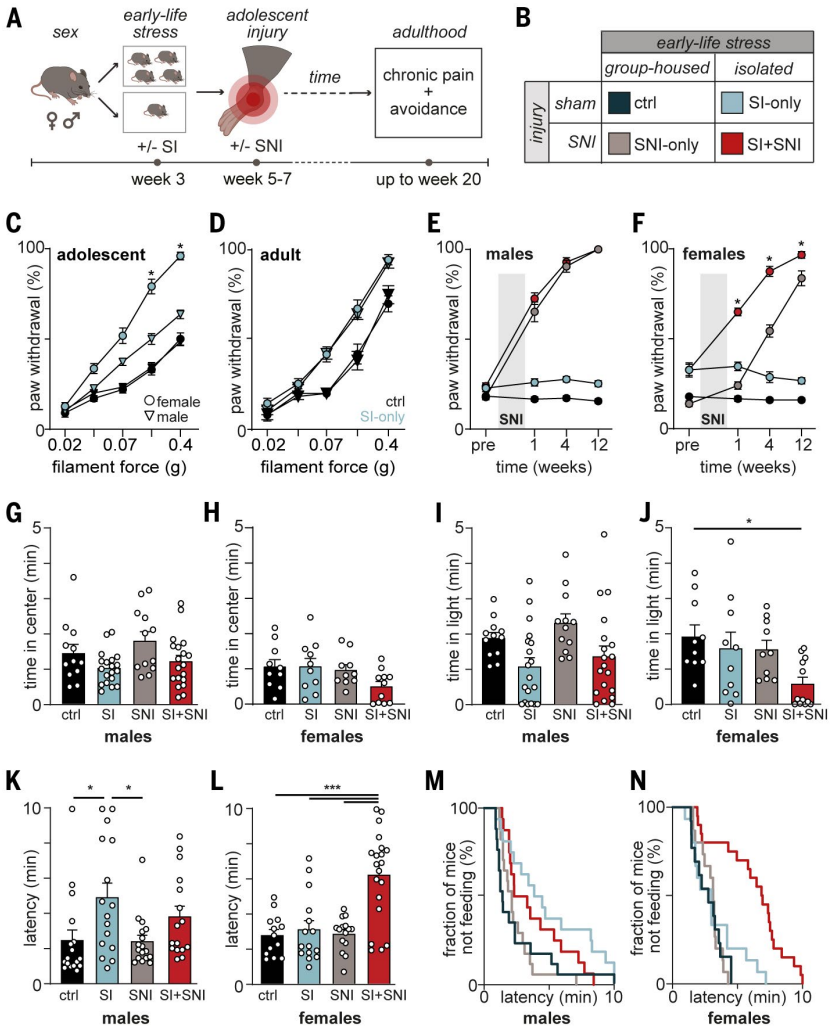


Fig. 1. Social isolation selectively exacerbates chronic neuropathic hypersensitivity and avoidance behavior in nerve-injured female mice. (**A** and **B**) Experimental design and full factorial study design. (**C** and **D**) Effect of SI on withdrawal responsivity across von Frey forces in male and female ctrl and SI-only mice before (C) and 12 weeks after (D) sham surgery; Significance was assessed using repeated measures three-way ANOVA (sex × force × SI): sex × SI interaction, before surgery, $F_{1,47} = 8.26$, $P = 0.006$; 12 weeks after sham surgery, $F_{1,47} = 0.12$, $P = 0.73$; main effect of SI, both time points, $P < 0.0001$. (**E** and **F**) Withdrawal responsivity during the von Frey test (mean paw withdrawal across 0.02- to 0.07-g forces) before and after sham or SNI surgery in (E) males and (F) females. Significance was assessed using three-way ANOVA: sex × SI × SNI interaction, week 1, $F_{1,96} = 8.30$, $P = 0.005$; week 4, $F_{1,96} = 16.12$, $P = 0.0001$; and week 12, $F_{1,96} = 6.02$, $P = 0.016$. Post hoc comparisons are as follows: SI+SNI versus SNI-only, females, $P < 0.0001$; males, $P > 0.98$. (**G** and **H**) Center exploration during OFT in (G) males and (H) females. Significance was assessed using three-way ANOVA: sex × SI × SNI interaction, $F_{1,95} = 0.37$, $P = 0.55$. (**I** and **J**) Light avoidance in the LDB in (I) males and (J) females. Significance was assessed using three-way ANOVA: sex × SI × SNI interaction, $F_{1,96} = 0.35$, $P = 0.55$; post hoc comparison, females, ctrl versus SI+SNI, $P = 0.041$. (**K** to **N**) Avoidance behavior in the NSF task in [(K) and (M)] males and [(L) and (N)] females. Significance was assessed using three-way ANOVA: sex × SI × SNI interaction, $F_{1,121} = 6.91$, $P = 0.0097$. Corresponding survival curves are shown in (M) and (N). Group sizes are as follows: males, ctrl ($n = 12$; NSF: $n = 17$), SI-only ($n = 19$; NSF: $n = 16$), SNI-only ($n = 12$; NSF: $n = 17$), SI+SNI ($n = 19$; NSF: $n = 16$); females, ctrl ($n = 10$; NSF: $n = 13$), SI-only ($n = 10$; NSF: $n = 15$), SNI-only ($n = 10$; NSF: $n = 15$), SI+SNI ($n = 12$; OFT: $n = 11$; NSF: $n = 20$), unless otherwise indicated. Error bars are mean ± SEM. *$P < 0.05$, and ***$P < 0.001$.

Selective facilitation of the PVT→CeA pathway in SI+SNI females

Synaptic plasticity in the PVT→CeA pathway might mediate the interaction-dependent enhancement of pain and avoidance in SI+SNI females. To specifically target CeA-projecting PVT neurons, we stereotaxically injected AAVretro-mCherry into the CeA and detected retrograde mCherry expression in PVT neurons (Fig. 2A). PVT projections strongly innervate the lateral CeA [CeL; (*14*)]. To characterize synaptic transmission onto CeL neurons, we expressed channelrhodopsin-2 (AAV-ChR2-EYFP) in PVT neurons and prepared acute CeL slices containing ChR2-expressing PVT terminals (Fig. 2B and fig. S6). Brief light pulses evoked excitatory postsynaptic currents (EPSCs; fig. S7A) in most recorded CeL neurons across sex and condition (422 of 449, 94.0%; fig. S6E), suggesting a dense and unaltered functional PVT→CeL connectivity. These synaptic responses were abolished by CNQX (6-cyano-7-nitroquinoxaline-2,3-dione) and AP-V (2-amino-5-phosphonopentanoic acid) (fig. S7), and stimulation of PVT terminals evoked EPSCs with a short delay of 5.55 ± 0.07 ms, consistent with direct glutamatergic innervation of CeA neurons.

To determine whether SI+SNI induces sex-specific synaptic plasticity, we performed whole-cell patch-clamp recordings in brain slices from CeL neurons during optogenetic stimulation of PVT terminals (Fig. 2B). Neither SI, SNI, nor SI+SNI altered AMPAR (α-amino-3-hydroxy-5-methyl-4-isoxazolepropionic acid receptor)– or NMDAR (*N*-methyl-D-aspartate receptor)–mediated EPSC amplitudes or decay kinetics in either sex (fig. S8). To minimize variability, we calculated AMPA/NMDA ratios in individual CeL neurons, which remained consistent across groups in both sexes (fig. S8, E and F), suggesting unaltered postsynaptic function. To test whether SI+SNI alters presynaptic plasticity in the PVT→CeL pathway, we stimulated PVT axons with two light pulses and measured the paired-pulse ratio (PPR) of AMPAR-mediated EPSCs in CeL neurons. SI, SNI, and SI+SNI did not alter PPRs in males (Fig. 2, C and D). By contrast, SI+SNI selectively increased the PPR in females relative to all other groups (ctrl, SI-only, and SNI-only; Fig. 2, C and E), indicating that SI+SNI induces female-specific presynaptic facilitation in the PVT→CeL pathway. Because CeL neurons are heterogeneous (*33*, *34*), we performed post hoc labeling to identify somatostatin (SOM)– and PKCδ-positive subpopulations (fig. S9, A and B). In males, PPRs were similar across subpopulations and conditions (fig. S9C). In females, SI+SNI was associated with higher PPRs in both SOM- and PKCδ-positive neurons (fig. S9D), suggesting that presynaptic facilitation is not limited to a cellular subtype.

Sex-dependent intrinsic firing adaptations under SI+SNI

We next examined whether SI+SNI alters CeL excitability in a sex-specific manner. Current-clamp recordings from CeL neurons revealed two electrophysiological clusters corresponding to regular-spiking (RS) and late-firing (LF) neurons (*34*–*36*) (Fig. 2F and figs. S10 and S11). In SI+SNI males, firing responses of both RS and LF neurons were unchanged relative to ctrl mice (Fig. 2, G and H). In females, SI+SNI selectively reduced firing in RS neurons (Fig. 2, G and I). Across all female groups, this effect was primarily driven by SNI and most pronounced in SI+SNI females (Fig. 2J and fig. S12). LF neurons showed no comparable changes (Fig. 2K and fig. S13). Intrinsic membrane properties showed distinct sex-dependent adaptations: In SI+SNI males (fig. S12, A to F), RS neurons exhibited hyperpolarized resting membrane potentials alongside lower spike thresholds and

Downloaded from https://www.science.org on November 24, 2026

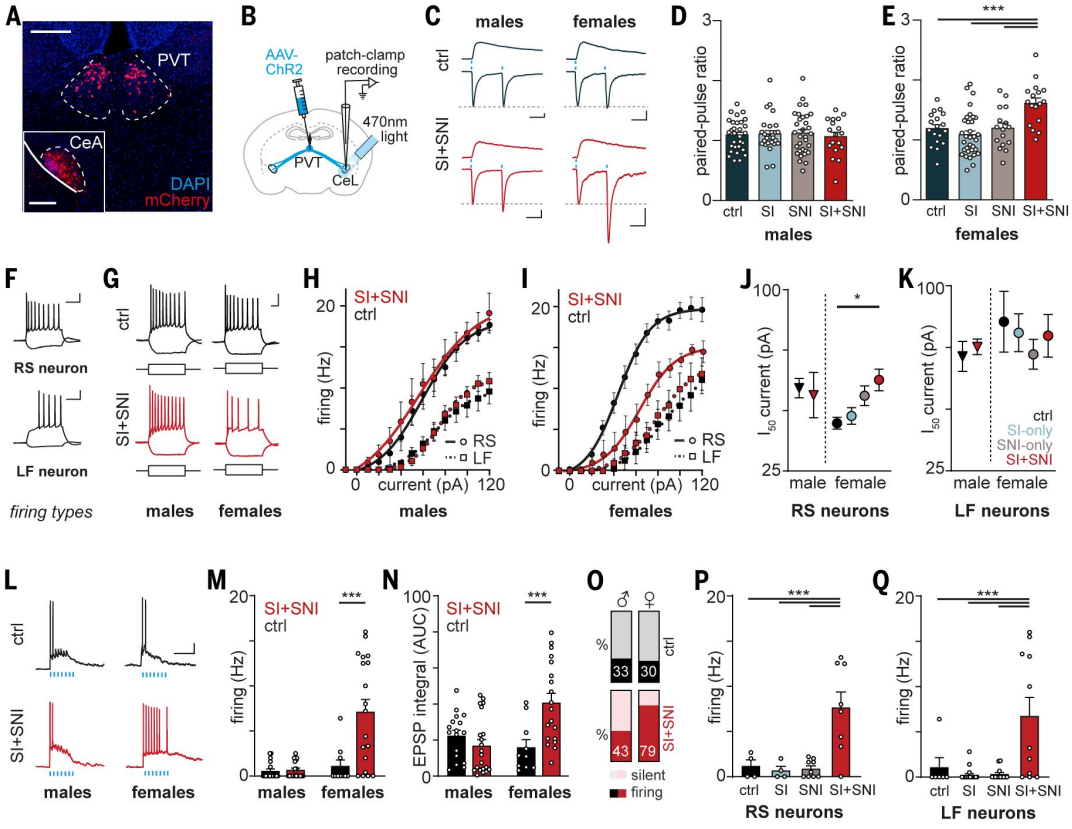


Fig. 2. SI+SNI selectively enhances activity-dependent PVT→CeL synaptic drive in female mice. (**A**) Retrograde labeling of PVT neurons projecting to the CeA after bilateral CeA injection of AAVretro-mCherry (inset). Scale bar is 300 μm. DAPI, 4′,6-diamidino-2-phenylindole. (**B**) Experimental schematic for optogenetic stimulation of PVT axons during whole-cell recordings from CeL neurons in acute slices. (**C**) Representative light-evoked EPSCs recorded at −70 mV and + 40 mV. Scale bars are 50 pA, 50 ms. (**D** and **E**) PPR of AMPAR-mediated EPSCs in CeL neurons from (D) males and (E) females. Significance was assessed using three-way ANOVA: sex × SI × SNI, $F_{1,183} = 9.13$, $P = 0.0029$. Tukey post hoc analysis is as follows: females, SI+SNI versus ctrl, SI-only, or SNI-only, $P = 0.0073$ to 0.0001. Sample numbers are as follows: males, ctrl ($n = 30$ cells from seven mice), SI-only ($n = 27$ from seven mice), SNI-only ($n = 32$ from seven mice), SI+SNI ($n = 18$ from five mice); females, ctrl ($n = 18$ cells from eight mice), SI-only ($n = 33$ from nine mice), SNI-only ($n = 16$ from four mice), and SI+SNI ($n = 17$ from four mice). (**F**) Representative firing patterns of RS and LF CeL neurons. (**G**) Example current-clamp recordings from RS neurons in male and female ctrl and SI+SNI mice at −50 pA and +50 pA current injections. (**H** and **I**) Frequency-current relationships of RS (circles) and LF (squares) CeL neurons in (H) males and (I) females. (**J** and **K**) Half-maximal firing current (I_{50}) for (J) RS and (K) LF neurons. For (J), significance was assessed using two-way ANOVA: sex × SI+SNI interaction, $F_{1,37} = 4.83$, $P = 0.034$. A follow-up two-way ANOVA was performed for females: SI × SNI interaction, $F_{1,36} = 0.23$, $P = 0.63$; main effect of SNI, $F_{1,36} = 12.51$, $P = 0.0011$; Tukey's post hoc test, ctrl versus SI+SNI, $P = 0.0033$. Sample numbers are as follows: males, ctrl ($n = 10$ from five mice), SI+SNI ($n = 7$ from four mice); females, ctrl ($n = 16$ from four mice), SI-only ($n = 6$ from two mice), SNI-only ($n = 10$ from three mice), SI+SNI ($n = 8$ from three mice). For (K), significance was assessed using two-way ANOVA: sex × SI+SNI interaction, $F_{1,65} = 0.38$, $P = 0.54$. A follow-up two-way ANOVA was performed for females: SI × SNI interaction, $F_{1,58} = 0.49$, $P = 0.49$. Sample numbers are as follows: males, ctrl ($n = 28$ from eight mice), SI+SNI ($n = 17$ from five mice); females, ctrl ($n = 11$ from four mice), SI-only ($n = 21$ from four mice), SNI-only ($n = 17$ from four mice), SI+SNI ($n = 13$ from three mice). (**L** to **N**) Effects of optogenetic burst stimulation of PVT inputs in CeL neurons. (L) shows representative traces. Shown in (M) is the burst-evoked action potential firing and in (N) cumulative depolarization (EPSP integral). Significance was assessed using two-way ANOVA with Sidak post hoc, sex × SI+SNI interaction: firing, $F_{1,63} = 11.83$, $P = 0.0010$; cumulative depolarization, $F_{1,63} = 12.25$, $P = 0.0009$. Sample numbers are as follows: males, ctrl ($n = 17$ from three mice), SI+SNI ($n = 21$ from five mice); females, ctrl ($n = 10$ from four mice), SI+SNI ($n = 19$ from three mice). AUC, area under the curve. (**O**) Proportion of CeL neurons generating action potentials during burst stimulation. Significance was assessed using Fisher's exact test, $P = 0.0148$. (**P** and **Q**) Burst-evoked firing of (P) RS and (Q) LF CeL neurons in female mice across groups. Significance was assessed using two-way ANOVA, SI × SNI interactions: RS neurons, $F_{1,21} = 8.28$, $P = 0.0090$; LF neurons, $F_{1,46} = 11.97$, $P = 0.0012$. Sidak post hoc test is as follows: SI+SNI versus ctrl, SI-only, or SNI-only, RS neurons, $P = 0.0102$ to 0.0007; LF neurons, $P = 0.0109$ to $P < 0.0001$. Sample numbers are as follow: RS neurons, ctrl ($n = 4$ from three mice), SI-only ($n = 4$ from two mice), SNI-only ($n = 9$ from two mice), SI+SNI ($n = 8$ from three mice); LF neurons, ctrl ($n = 6$ from four mice), SI-only ($n = 20$ from four mice), SNI-only ($n = 13$ from three mice), SI+SNI ($n = 11$ from three mice). Error bars are mean ± SEM. *$P < 0.05$, and ***$P < 0.001$.

increased spike amplitudes, consistent with compensatory intrinsic changes. In females (fig. S12, G to L), RS neurons showed hyperpolarized resting membrane potentials across SI-only, SNI-only, and SI+SNI mice, whereas rheobase increased only after SNI. Compensatory changes in the spike threshold and amplitude of RS neurons occurred in SNI-only females but were absent in SI+SNI females. These findings reveal sex-specific intrinsic adaptations, with compensatory mechanisms preserved in males but impaired in females, resulting in SNI-driven RS hypoexcitability that is most pronounced under SI+SNI conditions.

Enhanced facilitation increases PVT→CeA burst recruitment under SI+SNI

Paired pulse facilitation suggests increased functional PVT→CeL drive upon high-frequency input (*37*). We next recorded evoked firing and cumulative depolarization in CeL neurons during optogenetic burst stimulation of PVT axons in ctrl and SI+SNI mice of both sexes (Fig. 2L). In SI+SNI males, burst-evoked firing, cumulative depolarization, and the proportion of recruited CeL neurons were not altered. By contrast, SI+SNI females showed enhanced burst-evoked firing,

Downloaded from https://www.science.org on November 24, 2026

cumulative depolarization, and an increased fraction of recruited CeL neurons (Fig. 2, M to O). This enhancement was observed in both RS and LF neurons of SI+SNI females but not in ctrl, SI-only, or SNI-only mice (Fig. 2, P and Q). Together, these findings indicate that enhanced activity-dependent facilitation increases burst-evoked PVT→CeL drive in SI+SNI females, despite reduced intrinsic excitability of RS neurons, suggesting increased synaptic gain as a potential substrate for the female-specific pain-avoidance phenotype.

Stress-injury interaction drives anticipatory PVT→CeA hyperactivity

Because SI selectively amplified neuropathic pain, avoidance, and PVT→CeA plasticity in nerve-injured females, we focused on females in subsequent analyses. To investigate PVT→CeA activity during approach-avoidance conflict, we retrogradely expressed the calcium sensor GCaMP7c (AAV-DIO-GCaMP7c) in CeA-projecting PVT neurons and implanted optical cannulas above the PVT of female mice (Fig. 3, A and B, and fig. S14). We first examined basal PVT→CeA calcium dynamics and locomotor position during the OFT and NSF in ctrl females (Fig. 3, C to E). The OFT served as a control condition with no group differences in avoidance (Fig. 1H and fig. S15A). Cross-correlation analysis between calcium signals and center-directed position revealed a positive peak in the NSF, with PVT→CeA activity preceding movement by ~1.6 s (fig. S15, B and D). By contrast, no consistent coupling was observed in the OFT (fig. S15, C and D). Thus, PVT→CeA activity temporally precedes center-directed movement specifically during approach-avoidance conflict in the NSF. We next mapped high-amplitude calcium events (>3 SD above session mean) in CeA-projecting PVT neurons. Although mice displayed thigmotaxis in the OFT and NSF (Fig. 3, F and H, and fig. S15E), spatial patterns of PVT→CeA activity diverged (fig. S15F): High-amplitude events were concentrated in the corners during the OFT (Fig. 3G) but shifted to the center during the NSF (Fig. 3I). These findings indicate spatiotemporal, context-dependent recruitment of the PVT→CeA pathway during approach-avoidance conflict.

We then asked whether SI+SNI alters the context-dependent engagement of the PVT→CeA pathway. We analyzed the mean photometric activity across radial position during the OFT and NSF in all female groups (Fig. 3, J and K). During the OFT, SI+SNI females showed no changes in locomotion (fig. S15H) or PVT→CeA activity (Fig. 3J). By contrast, SI + SNI females displayed higher mean PVT→CeA activity near the NSF center relative to ctrl, SI-only, and SNI-only females (Fig. 3K), suggesting context-dependent PVT→CeA recruitment where approach-avoidance conflict is highest. Cross-correlation analysis further showed that in SI+SNI females, PVT→CeA activity remained uncoupled from locomotion in the OFT (Fig. 3L) but preceded movement by ~0.6 s in the NSF (Fig. 3M), suggesting anticipatory PVT→CeA activation during approach-avoidance conflict. To link these pathway dynamics with behavior, we quantified a "calcium slope" for each mouse, defined as the linear fit of mean calcium activity between the corner and center (fig. S15, I and J). Whereas OFT slopes were unrelated to behavior (Fig. 3N and fig. S15K), NSF slopes strongly correlated with avoidance latency (Fig. 3O and fig. S15G). Thus, SI+SNI selectively enhances anticipatory, context-dependent PVT→CeA activity during approach-avoidance conflict, providing a functional link between circuit engagement and avoidance in females.

The PVT→CeA pathway drives chronic pain and avoidance in females

To determine whether the PVT→CeA pathway causally mediates chronic neuropathic hyperalgesia and avoidance in female SI+SNI mice, we expressed the inhibitory designer receptor hM4Di or green fluorescent protein (GFP) in CeA-projecting PVT neurons (Fig. 4, A and C, and fig. S16). Three weeks later, mice received an intraperitoneal injection of clozapine-*N*-oxide (CNO; 3 mg per kg body weight) 45 min before

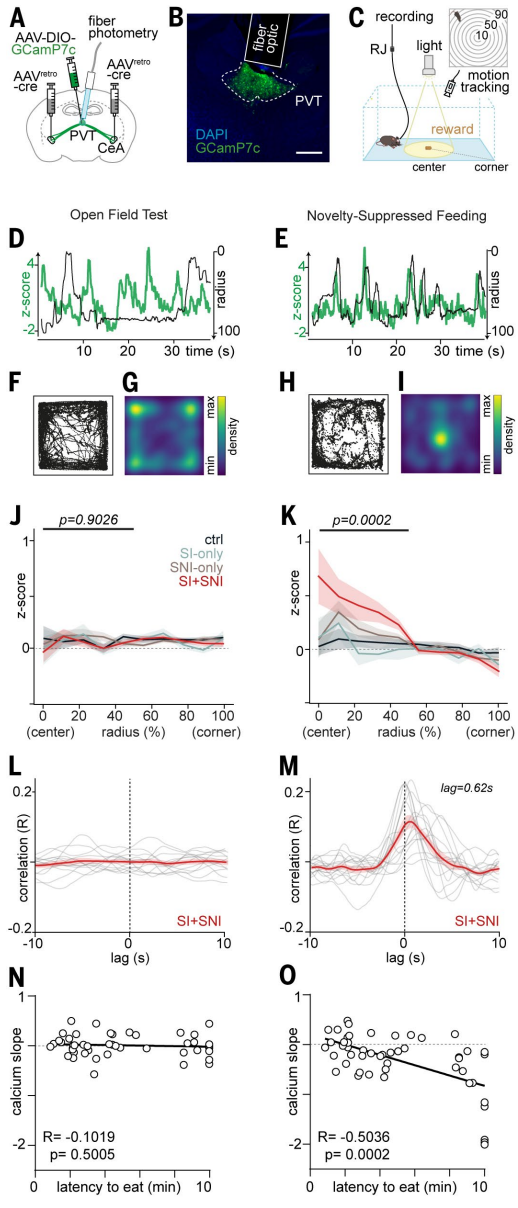


Fig. 3. Female SI+SNI mice show anticipatory PVT→CeA pathway hyperactivity during avoidance behavior. (**A**) Viral strategy for fiber photometric recordings from CeA-projecting PVT neurons. (**B**) GCaMP7c expression in PVT→CeA neurons. Scale bar is 200 μm. (**C**) Experimental setup for simultaneous photometry and behavioral tracking. The inset shows the polar transformation of arena coordinates. RJ, rotary joint. (**D** and **E**) PVT→CeA pathway activity aligned to kymographic position from the same mouse during the (D) OFT and (E) NSF. (**F** and **H**) Representative locomotor trajectories in the (F) OFT and (H) NSF. (**G** and **I**) Spatial probability density maps of high-amplitude calcium events (>3 SD above session mean) in female ctrl mice ($n = 14$) during the (G) OFT and (I) NSF. (**J** and **K**) Mean PVT→CeA calcium activity plotted as a function of radial location during the (J) OFT and (K) NSF. Significance was assessed using repeated measures two-way ANOVA: radius × group interaction, OFT, $F_{27,378} = 0.66$, $P = 0.90$; NSF, $F_{27,405} = 2.34$, $P = 0.0002$; post hoc comparison with Benjamini-Krieger-Yekutieli correction. Group sizes are as follows: ctrl (OFT: $n = 14$; NSF: $n = 15$), SI-only ($n = 6$), SNI-only ($n = 13$), SI+SNI mice (OFT: $n = 13$; NSF: $n = 15$). Shaded regions indicate mean ± SEM. (**L** and **M**) Cross-correlation between locomotion and PVT→CeA calcium activity in SI+SNI females during the OFT [(L); $n = 13$] and NSF [(M); $n = 15$]. Shaded regions indicate mean ± SEM. (**N** and **O**) Relationship between avoidance latency and calcium slope (center-to-corner-activity gradient) during the (N) OFT and (O) NSF. Spearman correlations with two-tailed *P* values are as follows: OFT [95% confidence interval (CI): −0.3884 to 0.2026, $n = 46$], NSF (95% CI: −0.692 to −0.251, $n = 49$).

Downloaded from https://www.science.org on November 24, 2026

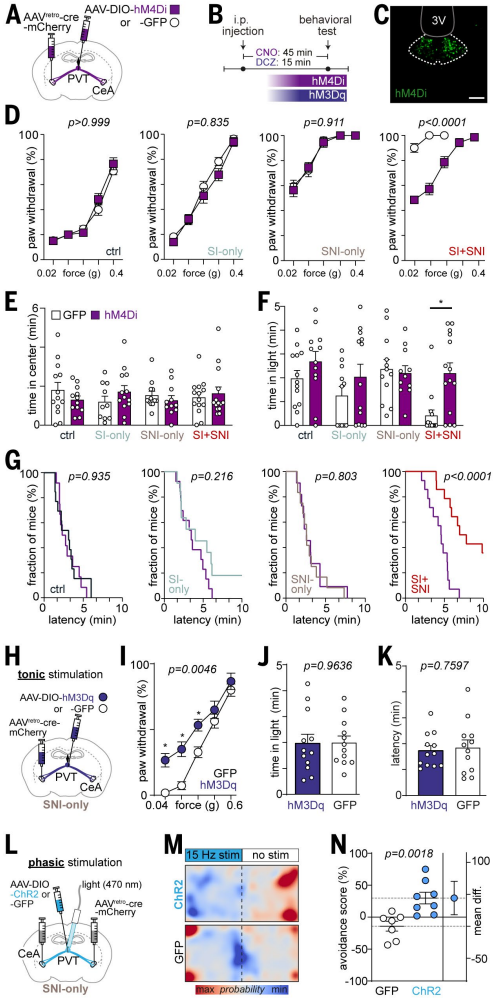


Fig. 4. The PVT→CeA pathway causally mediates enhanced pain and avoidance behavior in female SI+SNI mice. (**A**) Viral strategy for chemogenetic inhibition of the PVT→CeA pathway. (**B**) Experimental timeline. i.p., intraperitoneal. (**C**) Epifluorescence image showing expression of hM4Di-mCitrine in PVT→CeA neurons. Scale bar is 100 μm. (**D**) Chemogenetic inhibition of PVT→CeA neurons during the von Frey test 12 weeks after surgery in female hM4Di-expressing mice compared with female GFP-expressing mice. Significance was assessed using two-way ANOVA with Sidak post hoc test: hM4Di × group interaction, $F_{3,92} = 18.90$, $P < 0.0001$. (**E**) Time spent in the center zone during the OFT in female hM4Di-expressing mice compared with female GFP-expressing mice. Significance was assessed using two-way ANOVA: hM4Di × group interaction, $F_{3,91} = 1.231$, $P = 0.303$. (**F**) Chemogenetic PVT→CeA silencing during the LDB. Significance was assessed using two-way ANOVA: hM4Di × group interaction, $F_{3,92} = 3.971$, $P = 0.010$; Sidak post hoc test, SI+SNI, $P = 0.004$. (**G**) Chemogenetic PVT→CeA inhibition during the NSF. Survival curves and respective *P* values are shown. Significance was assessed using log-rank (Mantel-Cox) test with Bonferroni correction. Group sizes for (D) to (G) are as follows: hM4Di groups, ctrl ($n = 12$), SI-only ($n = 13$), SNI-only ($n = 11$), SI+SNI ($n = 14$); GFP groups, ctrl ($n = 13$), SI-only ($n = 11$), SNI-only ($n = 12$), SI+SNI ($n = 14$). (**H**) Viral strategy for chemogenetic activation of the PVT→CeA pathway. (**I** to **K**) Chemogenetic PVT→CeA activation 12 weeks after surgery in female hM3Dq-expressing mice ($n = 12$) compared with female GFP-expressing mice [$n = 11$ for (I); $n = 12$ for (J) and (K)]. Shown in (I) is the Von Frey test analyzed with a mixed-effects model (restricted maximum likelihood): hM3Dq × filament interaction, $F_{4,39} = 3.19$, $P = 0.0233$; Sidak post hoc comparison, 0.04 g, $P = 0.0037$; 0.07 g, $P = 0.001$; 0.16 g, $P = 0.0217$. The LDB (J) and NSF (K) were analyzed using unpaired *t* tests. (**L**) Viral strategy for optogenetic PVT→CeA stimulation in female SNI-only mice. (**M**) Representative probability heat maps showing spatial occupancy changes during real-time place avoidance (RTPA) in ChR2-expressing (top) and GFP-expressing (bottom) mice. (**N**) Quantification of light-evoked RTPA in ChR2-expressing ($n = 8$) and GFP-expressing ($n = 7$) mice. Significance was assessed using unpaired *t* test. Hedges' $g = 1.78$ (95.0% CI: 0.991 to 2.58).

behavioral testing (Fig. 4B). Chemogenetic inhibition of the PVT→CeA pathway selectively reduced mechanical withdrawal sensitivity in SI+SNI females in the von Frey test (Fig. 4D) but did not affect ctrl, SI-only, or SNI-only mice (Fig. 4D) or cold allodynia (fig. S17A). We concluded that PVT→CeA signaling is required for SI-dependent amplification of chronic neuropathic hypersensitivity but not for neuropathic pain driven by injury alone. Next, we assessed whether PVT→CeA signaling contributes to avoidance under SI+SNI conditions. Pathway inhibition did not alter exploration in the OFT in any group (Fig. 4E) but selectively reduced avoidance in SI+SNI females in the LDB (Fig. 4F and fig. S17B) and NSF (Fig. 4G), with no effects in ctrl, SI-only, or SNI-only mice. Pellet consumption after the NSF or locomotor activity in the OFT (fig. S17, C to E) were unchanged, excluding nonspecific motor or motivational effects. These findings demonstrate that PVT→CeA signaling is necessary for the pain-avoidance phenotype observed in SI+SNI females.

To test whether PVT→CeA signaling is sufficient to drive the pain-avoidance phenotype in the absence of SI, we expressed the excitatory designer receptor hM3Dq or GFP in CeA-projecting PVT neurons of female SNI-only mice (Fig. 4H and fig. S16). Three weeks later, mice received an intraperitoneal injection of deschloroclozapine (DCZ; 10 μg per kg body weight) 15 min before behavioral testing (Fig. 4B). Chemogenetic activation increased mechanical withdrawal sensitivity in the von Frey test (Fig. 4I), demonstrating that PVT→CeA activation is sufficient to enhance mechanical hypersensitivity under neuropathic conditions. PVT→CeA excitation did not alter gait parameters in ctrl females, excluding motor confounds (fig. S18). However, chemogenetic PVT→CeA activation did not increase avoidance in the LDB or NSF (Fig. 4, J and K), indicating that sustained PVT→CeA activation alone is insufficient to recapitulate the avoidance observed in SI+SNI females. Given the spatiotemporal PVT→CeA dynamics observed during the NSF, we next tested whether phasic PVT→CeA activation is sufficient to drive avoidance. We expressed ChR2 in CeA-projecting PVT neurons of female SNI-only mice (Fig. 4L and fig. S19, A to D) and performed a real-time place aversion assay. Phasic, chamber-contingent light stimulation induced robust avoidance of the stimulation-paired chamber relative to GFP controls (Fig. 4, M and N) without affecting locomotion (fig. S19, E and F). Thus, precise spatiotemporal activation of the PVT→CeA pathway is sufficient to drive real-time avoidance.

To assess projection specificity, we expressed hM4Di in PVT neurons projecting to the basolateral amygdala (BLA) of SI+SNI females (fig. S20, A to C). Unlike PVT→CeA inhibition, chemogenetic silencing of the PVT→BLA pathway increased paw withdrawal sensitivity (fig. S20D) without altering avoidance (fig. S20, E to G). Together, these findings identify functionally divergent PVT outputs and show that PVT→CeA signaling is both necessary and sufficient for amplifying mechanical hypersensitivity and conflict-driven avoidance after ELS and nerve injury in females.

Discussion

Our findings reveal a conditional, circuit-specific mechanism through which ELS selectively amplifies chronic pain and avoidance in adult female mice. Postweaning SI and SNI interact to drive a latent, activity-dependent gain state within the PVT→CeA pathway that remains silent at baseline but is unmasked by injury. This latent female-specific state is characterized by increased presynaptic facilitation, enhanced burst-evoked recruitment, and anticipatory pathway engagement during approach-avoidance conflict. Together, these findings extend existing models of central sensitization (*38*, *39*) by identifying a developmentally primed, projection-specific mechanism linking chronic pain and avoidance.

Previous stress-injury models reported female-biased pain phenotypes but differed in developmental timing and persistence (*40*, *41*). Here, postweaning SI combined with SNI during late adolescence produced a sustained, female-specific increase in neuropathic hypersensitivity.

Downloaded from https://www.science.org on November 24, 2026

This two-hit interaction extends beyond reflexive withdrawal to affective-motivational pain dimensions. Within this framework, pain expression in females appears dependent on developmental stage: Adolescent injury was associated with reduced early hypersensitivity, a pattern not observed after adult injury, whereas SI alone transiently increased hyperalgesia during adolescence before resolving with maturation. Prior work identified transient PVT→CeA contributions to early hypersensitivity in males that diminish at later stages of neuropathic pain (*20*, *42*). Here, we demonstrate sustained PVT→CeA involvement in the ELS-dependent amplification of chronic neuropathic pain in females. Chemogenetic inhibition selectively reduced the ELS-dependent pain enhancement without altering baseline injury-driven responses, indicating that this pathway mediates pain amplification rather than nociception. The absence of thermal pain modulation and dissociation from PVT→BLA projections further support a projection- and modality-specific involvement of the PVT→CeA pathway in pain processing.

Avoidance plays a central role in the maintenance of anxiety disorders and chronic pain (*3*). During approach-avoidance conflict, distinct PVT projections are differentially recruited (*18*, *43*, *44*). We identify exaggerated anticipatory PVT→CeA signaling as a circuit correlate of avoidance under SI+SNI conditions. Consistently, phasic optogenetic PVT→CeA activation was sufficient to drive avoidance, whereas chemogenetic excitation enhanced mechanical hypersensitivity without inducing avoidance, revealing a causal role for spatiotemporal PVT→CeA signaling in avoidance behavior. Unlike fear conditioning, which reorganizes specific CeA subpopulations (*14*, *45*), SI+SNI induced sex-specific PVT→CeA facilitation, not restricted to a CeL neuronal subtype, indicating a key role of enhanced PVT input drive. Paired-pulse facilitation is commonly interpreted as reflecting a lower initial release probability, which can selectively enhance synaptic transmission during burst firing (*37*). The SI × SNI interaction enhances PVT→CeA signaling despite the reduced intrinsic excitability of CeL RS neurons, indicating that burst-driven synaptic gain dominates circuit output and amplifies salient nociceptive or anxiogenic inputs. Although we identify a projection-specific mechanism linking ELS to female vulnerability to chronic pain, important limitations remain. The upstream mechanisms driving this sex-specific plasticity, and whether other forms of ELS induce similar effects, remain unknown.

Traditionally, central sensitization has been defined as an injury-driven increase in nociceptive gain arising from enhanced synaptic efficacy, increased excitability, and reduced inhibition (*38*). Our findings refine this view by identifying a developmentally primed, projection-specific gain state that remains silent until unmasked by subsequent injury. This extends central sensitization from an injury-triggered process to a state-dependent vulnerability mechanism linking diathesis-stress and fear avoidance models of chronic pain. Together, these insights suggest how childhood adversity can increase female vulnerability to chronic pain and comorbid anxiety in adulthood and identify a latent thalamo-amygdalar gain mechanism as a potential therapeutic target for reversing maladaptive sensitization after ELS.

REFERENCES AND NOTES

1. M. C. Bushnell, M. Čeko, L. A. Low, *Nat. Rev. Neurosci.* **14**, 502–511 (2013).
2. D. F. Tolin, E. B. Foa, *Psychol. Bull.* **132**, 959–992 (2006).
3. J. W. S. Vlaeyen, S. J. Linton, *Pain* **85**, 317–332 (2000).
4. K. Yamada *et al.*, *J. Pain Res.* **10**, 427–433 (2017).
5. C. Heim, C. B. Nemeroff, *Biol. Psychiatry* **49**, 1023–1039 (2001).
6. C. M. Kaplan *et al.*, *Nat. Rev. Neurol.* **20**, 347–363 (2024).
7. R. Gilbert *et al.*, *Lancet* **373**, 68–81 (2009).
8. G. E. Hodes, C. N. Epperson, *Biol. Psychiatry* **86**, 421–432 (2019).
9. L. A. McKibben *et al.*, *Pain* **166**, 2103–2115 (2025).
10. H. L. Goodwill *et al.*, *Neuropsychopharmacology* **44**, 711–720 (2019).
11. N. P. Bondar, A. A. Lepeshko, V. V. Reshetnikov, *Behav. Neurol.* **2018**, 1538931 (2018).
12. E. Candemir *et al.*, *Behav. Brain Res.* **369**, 111927 (2019).
13. A. P. Graf, A. C. Hansson, R. Spanagel, *Biol. Sex Differ.* **15**, 78 (2024).
14. M. A. Penzo *et al.*, *Nature* **519**, 455–459 (2015).
15. C. L. Kooiker, Y. Chen, M. T. Birnie, T. Z. Baram, *Biol. Psychiatry Glob. Open Sci.* **3**, 746–755 (2023).
16. Y. Zhu *et al.*, *Science* **362**, 423–429 (2018).
17. G. P. McNally, *Neurosci. Biobehav. Rev.* **125**, 193–207 (2021).
18. J. Ma *et al.*, *Nat. Neurosci.* **24**, 1429–1440 (2021).
19. F. H. Do-Monte, K. Quiñones-Laracuente, G. J. Quirk, *Nature* **519**, 460–463 (2015).
20. S.-H. Liang *et al.*, *J. Neurosci.* **40**, 7837–7854 (2020).
21. Y.-T. Chang *et al.*, *Pain* **160**, 1208–1223 (2019).
22. W.-K. Chen *et al.*, *J. Neurosci.* **30**, 10360–10368 (2010).
23. D. Li *et al.*, *Neuron* **113**, 2310–2324.e7 (2025).
24. T. J. Sharp, A. G. Harvey, *Clin. Psychol. Rev.* **21**, 857–877 (2001).
25. K. B. Jensen *et al.*, *Cereb. Cortex* **25**, 3903–3910 (2015).
26. G. J. Kirouac, *Front. Behav. Neurosci.* **15**, 627633 (2021).
27. C. L. Kooiker, M. T. Birnie, T. Z. Baram, *Front. Behav. Neurosci.* **15**, 673162 (2021).
28. P. Pliota *et al.*, *Mol. Psychiatry* **25**, 428–441 (2020).
29. R. E. Sorge *et al.*, *Nat. Neurosci.* **18**, 1081–1083 (2015).
30. V. Vacca *et al.*, *Sci. Rep.* **6**, 18980 (2016).
31. A. Muralidharan, S. G. Sotocinal, J.-S. Austin, J. S. Mogil, *Pain Rep.* **5**, e824 (2020).
32. P. N. Fuchs, C. T. McNabb, *J. Integr. Neurosci.* **11**, 61–72 (2012).
33. T. D. Wilson *et al.*, *Cell Rep.* **29**, 332–346.e5 (2019).
34. A. P. Adke *et al.*, *eNeuro* **8**, ENEURO.0402-20.2020 (2021).
35. S. Hunt, Y. Sun, H. Kucukdereli, R. Klein, P. Sah, *eNeuro* **4**, ENEURO.0367-16.2017 (2017).
36. W. Haubensak *et al.*, *Nature* **468**, 270–276 (2010).
37. S. L. Jackman, W. G. Regehr, *Neuron* **94**, 447–464 (2017).
38. A. Latremoliere, C. J. Woolf, *J. Pain* **10**, 895–926 (2009).
39. M.-A. Fitzcharles *et al.*, *Lancet* **397**, 2098–2110 (2021).
40. Y. Wang *et al.*, *Sci. Transl. Med.* **16**, eadj0395 (2024).
41. T. Nishinaka, K. Nakamoto, S. Tokuyama, *Life Sci.* **121**, 28–34 (2015).
42. Q.-Q. Tang *et al.*, *Neuropsychopharmacology* **49**, 455–466 (2024).
43. E. A. Choi, P. Jean-Richard-Dit-Bressel, C. W. G. Clifford, G. P. McNally, *J. Neurosci.* **39**, 4945–4958 (2019).
44. S. Beas *et al.*, *Curr. Biol.* **34**, 1549–1560.e3 (2024).

ACKNOWLEDGMENTS

We thank P. Tovote, L. L. Oettl, and R. Folkard for their critical feedback on earlier versions of the manuscript; A. Agarwal, C. Körber, A. Tappe-Theodor, R. Bernardi, and E. Roebel for their technical assistance and help during the establishment phase; A. Elsify for her support with graphic design; J. Tesarz and W. Eich for their support in planning; and R. Kuner for important infrastructural and project-specific support and critical feedback to the manuscript. The study was endorsed by the German Center for Mental Health (DZPG). **Funding:** This research was funded by the German Research Foundation (DFG) (SFB 1158 project B04 to S.W. and R.S., project B08 to T.Ku.; and TRR265 project A05 to R.S.). The authors acknowledge the data storage service SDS@hd, which is supported by the Ministry of Science, Research and the Arts Baden-Württemberg (M.W.K.) and the DFG through grant INST 35/1503-1 FUGG. **Author contributions:** Conceptualization: R.S., S.W.; Formal analysis: A.M.B., T.Ko., L.R., M.v.R., C.A.H., B.K., N.L., S.W.; Funding acquisition: R.S., S.W.; Investigation: A.M.B., T.Ko., L.R., M.v.R., C.A.H., B.K., C.C.-L., S.W.; Methodology: N.L., L.B., S.W.; Project administration: R.S., S.W.; Resources: H.-C.F., T.Ku., R.S., S.W.; Software: M.v.R., C.A.H., N.L., L.B.; Supervision: R.S., S.W.; Validation: S.W.; Visualization: A.M.B., T.Ko., C.A.H., L.R., M.v.R., N.L., S.W.; Writing – original draft: S.W.; Writing – review & editing: A.M.B., T.Ko., L.R., M.v.R., C.A.H., C.C.-L., N.L., H.-C.F., T.Ku., R.S., S.W. The first authorship of this paper is shared among five co-authors to accurately reflect their equal and substantial contributions to the research. Each of these authors played a pivotal role in distinct, yet complementary, aspects of the study. A.M.B. performed and analyzed behavioral and chemogenetic experiments. T.Ko. performed and analyzed electrophysiological experiments and discovered the sex-specific facilitation. L.R. performed fiber photometry experiments. M.v.R. first described the sex-specific avoidance in NSF, performed electrophysiological recordings, showed burst-driven enhancement, and analyzed photometric data. C.A.H. performed or analyzed electrophysiological, chemogenetic, and optogenetic experiments during the revision phase. **Diversity, equity, ethics, and inclusion:** Our study prioritized gender balance among first authors. Furthermore, we recognized sex as a critical biological variable and included both males and females, incorporating sex and sex-by-treatment interactions into our statistical models rather than collapsing across sexes. **Competing interests:** The authors declare that they have no competing interests. **Data, code, and materials availability:** All data generated or analyzed during this study are included in the article and the supplementary materials or stored and curated in public data repository at https://heibox.uni-heidelberg.de/d/f7aa69cc7f194240ad5e/. Custom-written codes and a demo dataset are available at https://github.com/WielandLab/Photometric_Spatial_Analysis. No new materials were generated in this study.

License information: Copyright © 2026 the authors, some rights reserved; exclusive licensee American Association for the Advancement of Science. No claim to original US government works. https://www.science.org/about/science-licenses-journal-article-reuse. This research was funded in whole or in part by DFG (SFB 1158 projects B04 and B08, TRR265 project A05, grant INST 35/1503-1 FUGG); as required, the author will make the Author Accepted Manuscript (AAM) version available under a CC BY public copyright license.

SUPPLEMENTARY MATERIALS

science.org/doi/10.1126/science.adx5757
Materials and Methods; Figs. S1 to S20; References (*45*–*56*); MDAR Reproducibility Checklist

Submitted 19 March 2025; resubmitted 7 April 2026; accepted 3 September 2026

10.1126/science.adx5757

Downloaded from https://www.science.org on November 24, 2026

Science
AAAS

A thalamo-amygdalar circuit drives female vulnerability to chronic pain after early-life stress

Anna Maria Borruto, Tabea Kohlund, Lukas Rettig, Martin von Renesse, Christian Alexander Hammer, Nikolas Leonhardt, Barbara Kurpiers, Claudia Calpe-López, Luca Benn, Hans-Christoph Friederich, Thomas Kuner, Rainer Spanagel, and Sebastian Wieland

Science **394** (6826), . DOI: 10.1126/science.adx5757

Editor's summary

Chronic pain in adults has been associated with early-life stress, particularly in women. Borruto *et al*. showed that in female mice, social isolation in young animals exacerbated pain sensitivity and anxiety-like behavior after nerve injury later in life. Electrophysiology and circuit perturbation experiments in vitro and in vivo showed that social isolation and nerve injury cooperatively increased the activation of the paraventricular thalamus-to-central amygdala pathway specifically in female animals. Blocking this activation prevented the increase in pain sensitivity and anxiety. The results provide a mechanistic link between early stress and chronic pain. —Mattia Maroso

View the article online

https://www.science.org/doi/10.1126/science.adx5757

Permissions

https://www.science.org/help/reprints-and-permissions

Downloaded from https://www.science.org on November 24, 2026

Use of this article is subject to the Terms of service

Science (ISSN 1095-9203) is published by the American Association for the Advancement of Science. 1200 New York Avenue NW, Washington, DC 20005. The title *Science* is a registered trademark of AAAS.

Copyright © 2026 The Authors, some rights reserved; exclusive licensee American Association for the Advancement of Science. No claim to original U.S. Government Works